

Radial Distribution Function for Semiflexible Polymers Confined in Microchannels

Patrick Levi and Klaus Mecke
Institut für Theoretische Physik,
Universität Erlangen-Nürnberg,
Staudtstraße 7, 91058 Erlangen, Germany

August 19, 2018

Abstract

An analytic expression is derived for the distribution $G(\vec{R})$ of the end-to-end distance \vec{R} of semiflexible polymers in external potentials to elucidate the effect of confinement on the mechanical and statistical properties of biomolecules. For parabolic confinement the result is exact whereas for realistic potentials a self-consistent ansatz is developed, so that $G(\vec{R})$ is given explicitly even for hard wall confinement. The theoretical result is in excellent quantitative agreement with fluorescence microscopy data for actin filaments confined in rectangularly shaped microchannels. This allows an unambiguous determination of persistence length L_P and the dependence of statistical properties such as Odijk's deflection length λ on the channel width D . It is shown that neglecting the effect of confinement leads to a significant overestimation of bending rigidities for filaments.

Bending of semiflexible macromolecules such as actin filaments play a crucial role for the mechanical properties of cells [1]. In general, the motion of biopolymers such as DNA or actin filaments takes place in gels or cytoplasm where sterical constraints forces a single molecule to bend in addition to the bending constantly induced by thermal motion. Advances in microfluidic techniques and in the direct visualization of actin filaments [2, 3, 4, 5, 6] make it nowadays possible to study experimentally the interplay of thermal fluctuations and confinement in controlled environments. Although the dynamics of single biomolecules can be measured for almost 20 years by fluorescence microscopy in simple confining geometries [7, 8, 9, 10] as well as

in microfabricated porous arrays [11, 12], the theoretical understanding of such constrained thermal motion is still hindered by the fundamental statistical problem to treat thermal activated undulations of macromolecules and steric repulsion from obstacles on the same analytical level. Whereas thermal bending modes can be treated well in Fourier space and steric constraints in real space, respectively, the combined interaction of thermal bending in confinement is not solved yet in a satisfactory way.

In order to characterize thermal fluctuations of polymers of length L one may calculate the tangent-tangent correlation function or the radial distribution function, i.e., the probability distribution $G(\vec{r})$ for the distance vector \vec{r} of the two filament ends [6]. Because end-to-end distances can be measured easily by labelling the ends of the macromolecule the latter served in the past as an important experimental tool to elucidate the physical properties of biopolymers including DNA in nanochannels [13]. However, estimated values for bending rigidity κ and persistence length $L_P = \kappa/(k_B T)$, for instance, depend on the details of confinement. An expression for $G(\vec{r})$ for freely fluctuating single, semiflexible polymers can be found in Ref. [14], which is unfortunately not applicable for confined and interacting filaments. The effect of confinement on the radial distribution function $G(\vec{r})$ is also relevant for the microrheology of actin solutions where entanglement plays an important role [15]. Thus, an analytical result for the dependence of $G(\vec{r})$ on confinement would provide an important tool to analyze experimental data in microfluidic devices in order to determine unambiguously the physical properties of biomolecules. The statistical mechanics of unconstrained fluctuations of semiflexible chain molecules ($L < L_P$) is well understood. A remarkable successful description is the worm-like chain model based on a fluctuating, elastic string [16]. However, not even the case of parabolic confinement was solved yet beyond tangent correlations functions [17]. Here, we present an analytic solution for the end-to-end distribution function for strong confinement with $D \ll L$ which is in quantitative agreement with experimental findings measured in Refs. [5, 6, 13], for instance. Moreover, a self-consistent ansatz allows the unambiguous mapping of non-parabolic confinements like hard walls or even van-der-Waals potentials on a quadratic Hamiltonian [18], so that our analytic result is even applicable on realistic substrate-filament interactions. This self-consistent ansatz was already successful in predicting the fluctuation spectrum of bounded membranes in excellent agreement with experimental data [18] as well as for thickness dependence of wetting layers [19]. Here, we present the first application on one-dimensional fluctuating filaments and compare our analytical result with experimental data for actin filaments [6].

Actin filaments have diameters of $\approx 8\text{nm}$, lengths of $L = 11 - 13\mu\text{m}$ and a

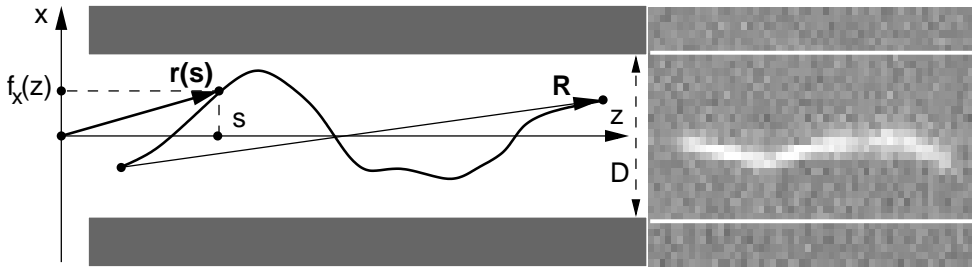


Figure 1: Microfluidic devices fabricated by soft photo-lithography makes it possible to observe thermal fluctuations of actin filaments in confining microchannels by fluorescence microscopy (image scanned from Ref. [6]). A theoretical description can be based on a Monge-parametrization of the perpendicular deviation $f(z)$ of the filament from the z -axis along the channel instead of its arc length s . Despite the limited spatial resolution of the image the end-to-end distance \vec{R} can be measured accurately which makes its distribution $G(\vec{R})$ an ideal quantity to determine physical parameters of the filament. $G(\vec{R})$ is given analytically in Eq. (3) in very good agreement with experimental data shown in Fig. 3.

persistence length of about $L_P \approx 15\mu\text{m}$ yielding thermal fluctuations which can be observed by optical fluorescence microscopy [6]. Thus, in addition to the importance of these thermal fluctuations for the biological functioning of cells, actin filaments can be used as an experimentally accessible model system for semiflexible polymers where $L < L_P$. The statistical properties of confined filaments depend crucially on the ratio L/λ of the total length L of the filament to Odijks deflection length λ which equals approximately the number of bendings caused by the walls. Because the channel width D in the experiments described in Ref. [6] is much smaller than the length of the macromolecules we focus here on the strong confinement limit $D \ll L$. An actin filament of length L is modelled as a differentiable curve in space parametrized by the position vector $\vec{r}(s)$ and the arc length $s \in [0, L]$ (see Fig. 1). Because polymers in microchannels are elongated as shown in the fluorescence microscopy image, one may ignore loops or overhangs of $\vec{r}(s)$. Applying a Monge parametrisation one can write the thermally induced deviation $\vec{f}(z) = (f_x(z), f_y(z))$ from the z -axis \vec{e}_z parallel to the channel walls as single-valued functions, i.e., $\vec{r}(s) = (\vec{f}(z), z)$. Then, the Hamiltonian of an elastic string with bending rigidity κ can be written as

$$\mathcal{H}_{\text{bend}} = \frac{\kappa}{2} \int_0^L ds \left(\frac{\partial \vec{t}}{\partial s} \right)^2 = \frac{\kappa}{2} \int_0^{L_z} dz \frac{(\partial_z \vec{t}(z))^2}{\sqrt{1 + (\partial_z \vec{f})^2}} \quad (1)$$

with the normalized tangent vector $\vec{t}(s) = \frac{\partial \vec{r}}{\partial s} = (\partial_z \vec{f}, 1) / \sqrt{1 + (\partial_z \vec{f})^2}$, the abbreviation $\partial_z = \frac{\partial}{\partial z}$, and the projection L_z of the contour length L on the z -axis of the channel. Notice, that $L_z(\vec{f})$ itself is a function of \vec{f} given by the implicit relation $L = \int_0^{L_z(\vec{f})} dz \sqrt{1 + (\partial_z \vec{f}(z))^2}$ at fixed contour length L . The channel walls are assumed to be purely repulsive with a quadratic cross-section and width D . To model the confinement we add an energy term $\mathcal{H}_{\text{pot}} = \frac{1}{2} \int_0^{L_z} dz U(\vec{f}(z))$ where the potential U describes the interaction of the filament with the substrate material.

In order to avoid non-Gaussian path integrals in the beginning, we start with a parabolic potential $U(\vec{f}) = \frac{E}{2} \vec{f}^2$ perpendicular to the channel axis \vec{e}_z . In a second step we map self-consistently non-Gaussian potentials on an effective parabolic potential strength E and derive an explicit expression for the dependence of E on the channel width D . Accordingly, we expand also $\mathcal{H}_{\text{bend}}$ up to second order in \vec{f} because the fluctuations $f_{x,y}(z)$ are expected to be small at room and even physiological temperatures, yielding $\mathcal{H} = \mathcal{H}_{\text{bend}} + \mathcal{H}_{\text{pot}} = \frac{1}{2} \int_0^{L_z} dz \left[\kappa (\partial_z \vec{f})^2 + E \vec{f}^2 \right]$. Thus, the statistical properties of the actin filament are determined by only two characteristic length scales, the persistence length $L_P = \kappa / (k_B T)$ and the deflection length $\lambda = \xi_{\parallel} = \sqrt[4]{\frac{4\kappa}{E}}$ introduced by Odijk [17]. Whereas L_P is a quantitative measure for the thermal flexibility of the filament, λ is the characteristic length of bendings forced by the confinement. The Gaussian approximation is additionally justified by the channel confinement which suppresses effectively large fluctuations on length scale larger than λ . Notice, that the inextensibility constraint $|\vec{t}| = 1$ is violated in the Gaussian approximation, although automatically fulfilled by using the arc length s in $\vec{t} = \frac{\partial \vec{r}}{\partial s}$.

We exploit open end boundary conditions and mirror the polymer at the origin in order to be able to apply periodic boundary conditions for this augmented configuration. The mirroring of the polymer suppresses sine-modes but doubles the cosine-modes by allowing wavevectors $\frac{\pi}{L} k$ ($k \in \mathbb{N}$) instead of $\frac{2\pi}{L} k$ as for usual periodic boundary conditions. By doing so, the end and the midpoint of the periodic string, i.e. the two endpoints of the original filament can fluctuate freely and are not constrained on the same excursion, which is crucial for the following analytic calculation. This boundary condition is equivalent to the one used by Wilhelm and Frey for unconfined polymers [14], so that we recover their result for $E = 0$ as one can see below. Then, $\vec{f}(z)$ can be expressed in a discrete Fourier sum $f_{x,y}(z) = \sum_{k=1}^{\infty} \tilde{f}(k) \cos\left(\frac{\pi}{L_z} k z\right)$ with integer k . The end-to-end vector $\vec{R} = \int_0^L ds \vec{t}(s)$

reads in Gaussian approximation in terms of the Fourier amplitudes

$$\vec{R} = L\vec{e}_z - \sum_{k=1}^{\infty} \begin{pmatrix} (1 - (-1)^k)\tilde{f}(k) \\ Lk^2\tilde{f}(k)^2/4 \end{pmatrix} + \mathcal{O}(\tilde{f}(k)^4) \quad (2)$$

yielding the end-to-end distribution function $G(\vec{r}) = \langle \delta(\vec{r} - \vec{R}) \rangle = \delta(r_x)\delta(r_y)G_0(r)$ where the angle brackets indicate an ensemble average determined by the Hamiltonian (1) in Gaussian approximation. Applying Fourier expansion of $\delta(\vec{r} - \vec{R})$ as well as residuum theorem one finds

$$\begin{aligned} G_0(r) &= \frac{1}{L\mathcal{N}} \sum_{k=1}^{\infty} e^{F(k)(r/L-1)} F(k) \prod_{k' \in \mathbb{N} \setminus \{k\}} \frac{F(k')}{F(k') - F(k)} \\ &= \frac{L_P}{\mathcal{N}L^2} \sum_{k=1}^{\infty} e^{F(k)(\frac{r}{L}-1)} \frac{\pi^2 k (-1)^{k-1}}{\sin \frac{\pi k_c^2}{k}} \left(1 - \frac{k_c^4}{k^4}\right) \end{aligned} \quad (3)$$

with the dimensionless length ratios

$$k_c^4 = \frac{4}{\pi^4} \frac{L^4}{\lambda^4} \quad \text{and} \quad F(k) = \frac{L_P}{L} \pi^2 k^2 \left(1 + \frac{k_c^4}{k^4}\right). \quad (4)$$

An essential step in the derivation of this analytic result is the splitting of the product

$$\prod_{k' \neq k} \frac{F(k')}{F(k') - F(k)} = \prod_{k' \neq k} \frac{k'^2}{k'^2 - k^2} \prod_{k' \neq k} \frac{1 + \frac{k_c^4}{k'^4}}{1 - \frac{k_c^4}{k'^2 k^2}} \quad (5)$$

into two factors. The first product equals $(-1)^{k-1}$ whereas the second one can be rewritten in terms of the functions $p_n(x) = \prod_{j=1}^{\infty} \left(1 + \frac{x}{j^4}\right)$ with $p_2(x) = \frac{\sin(\pi\sqrt{-x})}{\pi\sqrt{-x}}$. Because $p_4(k_c^4)$ is a numerical factor independent on k , it can be put into the normalization constant \mathcal{N} which is determined by $\int d^3r G(r) = 1$.

In Fig. 2 we illustrate the dependence of $G_0(r)$ on the potential strength E as well as on the bending rigidity κ , i.e., on λ and L_P , respectively. We observe that with increasing E the most probable end-to-end distance r/L , i.e., the position of the peak in $G_0(r)$ is shifted to higher values and that the peak gets sharper. This is obvious since strong confinement supports rather straight conformations and short end-to-end distances get more unlikely. In the limit of vanishing confinement $E \rightarrow 0$ one finds a diverging deflection

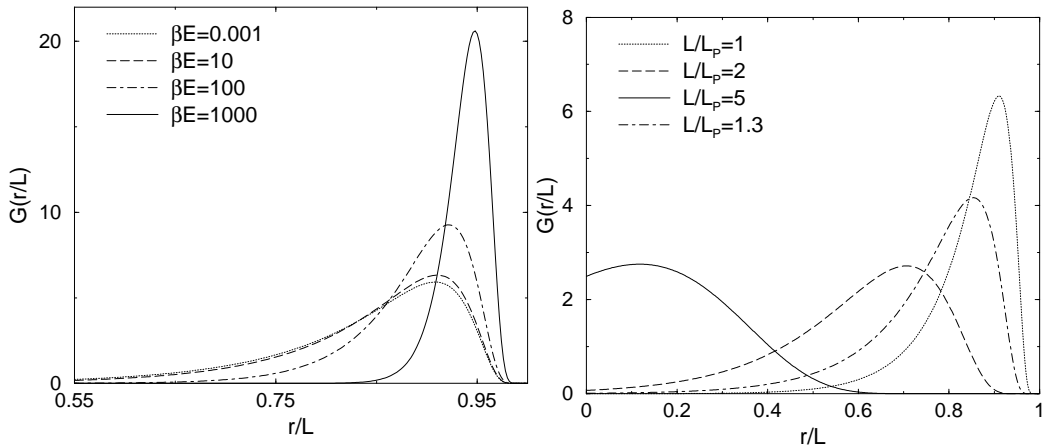


Figure 2: Radial distribution function $G_0(R)$ for filaments of persistence length L_P as function of the confining potential strength E and the contour length L .

length $\lambda \rightarrow \infty$ and a vanishing critical wavevector $k_c \rightarrow 0$. In this limit, Eq. (3) is identical to the result of Wilhelm and Frey derived for freely fluctuating semiflexible polymers [14] where large wavevectors k do not contribute significantly to $G_0(r)$ due to bending energies. However, the channel walls induce an apparent larger stiffness as shown in Fig. 2. Thus, analyzing experimental data with the result presented in Ref. [14] would lead to significant larger values for the persistence length of the polymer. Finite values of the potential strength E , i.e., of k_c effectively suppress additionally wavevectors with $k < k_c$ in the radial distribution function, so that only modes with $k \approx k_c$ contribute significantly to the partition sum.

In order to compare the explicit expression for the radial distribution $G(r)$ given by Eq. (3) to experimental data we need to relate the average projection length $\langle L_z \rangle$ to the contour length L . In Gaussian approximation one finds $\langle L_z \rangle = L/(1 + \sigma'^2)$ with the variance

$$\sigma'^2 = \langle (\partial_z f_{x,y})^2 \rangle = \int_0^{q_{\max}} \frac{dk}{\pi} \frac{k_B T k^2}{E + \kappa k^4} \quad (6)$$

of the first derivative of the filament position \vec{f} with respect to the lateral position z . The upper border of the integral σ'^2 $q_{\max} = 2\pi/\xi$ where ξ denotes the length scale where thermal fluctuations disappear, which is either the monomer length of the considered protein or the spatial resolution of the experimental setup as in our case. Evaluating data from microscopy experiments one does not measure the contour length L of the filament but only the

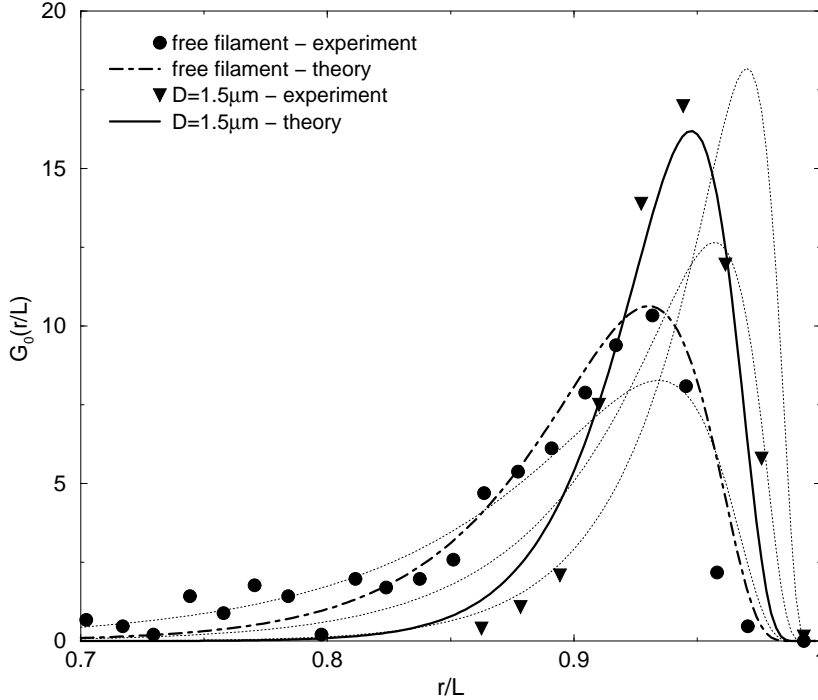


Figure 3: The analytical result for the radial distribution function $G_0(r)$ given by Eq. (3) (solid line) describes accurately the measurements of the end-to-end distance of the filaments by fluorescence microscopy (symbols, see Ref. [6]). We find consistently the persistence length $L_p \approx 15 \pm 3\mu$ for all measurements whereas a theory neglecting confinement (dotted lines with $E = 0$ and $\kappa = 19, \kappa = 25, \kappa = 35$) does not agree with the experimental data. Moreover, comparing the data and the theory without confinement ($E = 0$) would imply a dependence of the persistence length on the channel width D .

projection $L_{||}$ of L on the focal plane. Analogous to L_z one finds in Gaussian approximation for the averages the relation $\langle L_z \rangle = \langle L_{||} \rangle / (1 + \sigma'^2/2)$ which is used in Eq. (3) when comparing experimental data with the theoretical result. Notice, that this correction remedies the violation of the inextensibility constraint $|\vec{t}(s)| = 1$ within Gaussian approximation.

In Fig. 3 we compare the theoretical expression (3) to experimental distributions measured by fluorescence microscopy from a single actin filament in a microchannel. The data and description of the experimental setup can be found in Ref. [6]. The widths of the channels range from $D = 1.5\mu\text{m}$ over $D = 5.8\mu\text{m}$ to almost infinite widths where the filament lengths are in general larger than $10\mu\text{m}$. We fit the end-to-end distribution function (3) using the

potential strength E and the bending rigidity κ as free parameters and find quantitative agreement between the theoretical prediction for confinement and the experimental data. In all cases we find consistently the persistence length $L_P \approx 15 \pm 3 \mu\text{m}$ in good agreement with $L_P = 18 \mu\text{m}$ from Ref. [6] considering the difficulties in measuring persistence lengths. It is important to notice that the agreement between theory and experiment for different channel widths is found for identical persistence length L_P . Without taking the effect of confinement into account, i.e., a finite value for k_c in Eq. (3) one would obtain significant different values for L_P . Fig. 3(a) shows also that an unconfined filament ($E = 0$) cannot be used to describe the data. Taking the height of the peak would systematically overestimate the persistence length and lead to unrealistic values. The quality of the fits with finite E indicates that an effective parabolic potential is appropriate, if the strength E depends on the channel geometry. Here the channel geometry is set by a rectangular cross-section with width $D_1 = D$ and height $D_2 \approx 1.4 \mu\text{m}$. In a final step we derive an analytic expression to map the channel geometry on a parabolic potential with $E(D_1, D_2)$ which can be used in Eq. (3) even for non-parabolic confinement of the filament.

For hard wall confinement in a channel with rectangular cross-section the potential reads $U^{(hw)}(\vec{f}) = U_x(f_x)U_y(f_y)$ with $U_i(f_i) = 0$ for $-\frac{D_i}{2} < f < \frac{D_i}{2}$ and $U_i(f_i) = \infty$ otherwise. To do the mapping we employ a technique from Ref. [18] which proved to work well for two dimensional membranes and thin films [19]. It considers the root mean square fluctuations amplitude $\sigma_{x,y}^2 = \langle f_{x,y}^2 \rangle$ given by $\sigma^{-2} = 2^{3/2} \beta \kappa^{1/4} E^{3/4}$ for parabolic confinement.

The central idea is to calculate σ^2 separately in Fourier space for short wavelength fluctuations and in real space for long wavelengths, respectively, and assuming that both approaches lead to the same value. In real space the polymer is to this end divided into independently fluctuating segments of size ξ_{\parallel} . This self-consistent ansatz leads to the implicit equation

$$0 = \int_{-\infty}^{\infty} df (f^2 - \sigma_{x,y}^2) e^{-\beta U_{x,y}(f) \xi_{\parallel} - \frac{f^2}{2\sigma_{x,y}^2}}. \quad (7)$$

for the fluctuation amplitude $\sigma_{x,y}$. Here, $\xi_{\parallel} = \lambda = \sqrt[4]{\frac{4\kappa}{E}}$ is the correlation length parallel to the channel given by the deflection length λ . In case of the hard wall potential $U^{(hw)}$ we arrive at the equation $\exp(-1/(16\mu)) = \sqrt{\pi\mu} \text{erf}(1/\sqrt{16\mu})$ for the ratio $\mu = \sigma^2/D^2$. Because $\mu \approx 0.063777$ is constant, one finds the scaling $\sigma \propto D$ analogous to Odijk's scaling relation $\lambda \propto L_P^{1/3} D^{2/3}$ derived for spherical channels [17]. Moreover, one can determine the prefactor analytically by applying $4\beta E L_P^{1/3} \mu^{4/3} D^{8/3} = 1$ yielding the

expression

$$\lambda = \sqrt[4]{\frac{4\kappa}{E}} = 2L_P^{\frac{1}{3}}\sigma^{\frac{2}{3}} = 2\mu^{\frac{1}{3}} L_P^{1/3} D^{2/3} \quad (8)$$

for the deflection length. Notice, that for a one dimensional filament the ratio $\mu = \sigma^2/D^2 \approx 0.063777$ is much smaller compared to the value $\mu \approx 0.2$ for a two dimensional membrane [18].

Computing E for the parameters of the measured data set shown in Fig. 3 we find a good agreement with the experimental data, which makes our explicit result an important tool to analyse biophysical in vitro studies where more complex constraints are relevant due to the biological environments. For instance, spatial constraints can not only be induced by solid channel walls but also by forces between parallel filaments within the channel. Repulsive forces lead to additional extension whereas attractive interactions may cause the formation of bundles of semiflexible filaments. Our analytical self-consistent approach seems to exhibit a discontinuous unbinding transitions of bundles recently found in Monte-Carlo simulations [20]. Also in steady shear flow the conformational dynamics of individual polymer molecules can be visualised and the probability distribution for the polymer extension can be measured [21, 22]. The explicit expression (3) for the radial distribution function may be applied to distinguish between extensions due to shear flow or due to spatial confinement in channels. Recently, the fluctuations of semiflexible polymers were visualised in a nematic liquid crystal where confinement due to rod-like colloidal particles leads to an elongation of the filament [23]. The observed coil-rod transition makes our approach applicable so that the explicit expression for the radial distribution function may be used to describe the elongation of the filaments beyond the tangent correlation function used in Ref. [23]. We expect that our main result, the explicit expression for $G(\vec{R})$, can be used to analyze experiments of more complex situations such as solutions of filaments even in inhomogeneous channel geometries which is crucial for the understanding of the cytoskeleton in vivo.

References

- [1] A.R. Bausch and K. Kroy, *Nature Physics* **2**, 231 (2006).
- [2] F. Gittes, B. Mickney, J. Nettleton, and J. Howard, *J. Cell Bio* **120**, 923 (1993).
- [3] A. Ott et al., *Phys. Rev. E* **48**, R1642 (1993).
- [4] J. Käs, H. Strey, and E. Sackmann, *Nature* **368**, 226 (1994).

- [5] L. Goff, O. Hallatschek, E. Frey, and F. Amblard, *Phys. Rev. Lett.* **89**, 258101 (2002).
- [6] S. Köster, D. Steinhauser, and T. Pfohl, *J. Phys. Cond. Mat.* **17**, S4091 (2005).
- [7] T. W. Houseal, C. Bustamante, R. F. Stump, M. F. Maestre, *Biophys. J.* **56**, 507 (1989).
- [8] M. Matsumoto et al., *J. Polym. Sci. B Polym. Phys.* **30**, 779 (1992).
- [9] T. T. Perkins, D. E. Smith, S. Chu, *Science* **264**, 819 (1994).
- [10] C. Bustamante, Z. Bryant and S. B. Smith, *Nature* **421**, 423 (2003).
- [11] J. Han and H. G. Craighead, *Science* **288**, 1027 (2000).
- [12] D. Nykypanchuk, H. H. Strey, and D. A. Hoagland, *Science* **297**, 987 (2002).
- [13] J. O. Tegenfeldt, et al. *PNAS* **101**, 10979 (2004).
- [14] J. Wilhelm and E. Frey, *Phys. Rev. Lett.* **77**, 2581 (1996).
- [15] M. Gardel et al., *Phys. Rev. Lett.* **91**, 158302 (2003).
- [16] O. Kratky and G. Porod, *Recl. Trav. Chim. Pays-Bas Belg.* **68**, 1106-1123 (1949).
- [17] T. Odijk, *Macromolecules* **16**, 1340 (1983).
- [18] K. Mecke, T. Charitat, and F. Graner, *Langmuir* **19**, 2080 (2003).
- [19] J. Vorberg, St. Herminghaus, and K. Mecke, *Phys. Rev. Lett.* **87**, 196105 (2001).
- [20] J. Kierfeld, T. Kühne, and R. Lipowsky, *Phys. Rev. Lett.* **95**, 038102 (2005).
- [21] D. Smith, H. Babcock, S. Chu, *Science* **283**, 1725 (1999).
- [22] C. M. Schroeder, H. P. Babcock, E. S. G. Shaqfeh, and S. Chu, *Science* **301**, 1515 (2003).
- [23] Z. Dogic et al., *Phys. Rev. Lett.* **92**, 125503 (2004).